

Daytime and Nighttime Polar Cloud and Snow Identification Using MODIS Data

Qing Trepte
SAIC, Hampton, VA USA

Patrick Minnis
Atmospheric Sciences, NASA Langley Research Center, Hampton, VA USA

Robert F. Arduini
SAIC, Hampton, VA USA

Extended Abstract for
*SPIE 3rd International Asia-Pacific Environmental Remote Sensing Symposium 2002:
Remote Sensing of the Atmosphere, Ocean, Environment, and Space*
Hangzhou, China
October 23-27, 2002

Daytime and nighttime polar cloud and snow identification using MODIS data

Qing Z. Trepte*^a, Patrick Minnis^b, Robert F. Arduini^a

^aScience Applications International Corp.; ^bAtmospheric Sciences, NASA Langley Research Center

ABSTRACT

The Moderate Resolution Imaging Spectroradiometer (MODIS) on Terra, with its high horizontal resolution and frequent sampling over Arctic and Antarctic regions, provides unique data sets to study clouds and the surface energy balance over snow and ice surfaces. This paper describes a polar cloud mask using MODIS data. The daytime cloud and snow identification methods were developed using theoretical snow bi-directional reflectance models for the MODIS 1.6 and 3.75- μm channels. The model-based polar cloud mask minimizes the need for empirically adjusting the thresholds for a given set of conditions and reduces the error accrued from using single-value thresholds. During night, the MODIS brightness temperature differences (BTD) for 3.75 - 11, 3.75 - 12, 8.55 - 11, and 6.7 - 11 μm are used to detect clouds while snow and ice maps are used to determine snow and ice surfaces. At twilight, the combination of the 1.6- μm reflectance and the 3.75 - 11- μm BTD are used to detect clouds. Examples of the cloud mask results from daytime, nighttime, and twilight data show good agreement with visual interpretation of the imagery. Comparisons of the modeled and observed reflectances for clear snow areas reveal good agreement at 1.6 μm , but 10 - 35% overestimates of the 3.75- μm reflectance by the model. Over the Arctic, the modeled visible reflectance is significantly greater than the observed values. Better agreement is obtained over the Antarctic where snow melt is less significant.

Key words: MODIS, snow reflectance, polar cloud mask, near-infrared, Arctic, Antarctica, CERES, clouds

1. INTRODUCTION

Accurate quantification of the surface and top-of-atmosphere (TOA) radiation budget from satellite radiance data requires discrimination of the cloudy and clear areas within a given scene. The Clouds and Earth's Radiant Energy System (CERES) combines broadband radiances with high spatial resolution narrowband imager data to determine the components of a given broadband field of view and retrieve an accurate flux from the radiance [1]. Scene identification over polar regions is difficult because clouds are often similar to the underlying surface in terms of temperature and visible reflectance. During the day, however, the BTD between the 3.75 and 11- μm channels is greater for clouds than for clear snow allowing for discrimination between clouds and snow. This difference is in the reflected solar component of the solar infrared (SIR) 3.75- μm channel. Similarly, clouds are usually more reflective than snow at 1.6 μm , a near-infrared (NIR) channel. Typically, these channels are used for detecting clouds and snow based on empirically based thresholds. These empirical thresholds are less than satisfactory because of their wide variability, especially with viewing and illumination angles. To facilitate more accurate automated scene identification over snow-bound regions, better characterizations of the bi-directional reflectance patterns of snow at 0.65, 1.6 and 3.75 μm are developed and incorporated in the daytime clouds and snow detection. Theoretical surface emissivities are derived for application to the nighttime polar mask. By using theoretically based polar masks, it should be possible to consistently detect clouds over the Arctic, Antarctica, and other snow-covered areas using a variety of different satellites. The polar mask developed here is for use in the CERES cloud retrieval algorithms and for application to Advanced Very High Resolution data processed for the Atmospheric Radiation Measurements (ARM) Program. This paper describes the development of the CERES mask and examines the validity of the theoretical models used to define the clear-sky conditions.

* Corresponding author address: Q. Z. Trepte, SAIC, 1 Enterprise Parkway Center, Hampton, VA 23666 USA
Email address: q.z.trepte@larc.nasa.gov

2. METHODOLOGY

2.1 Theoretical models and clear-sky conditions

Detection of clouds often requires a reasonable estimate of the expected radiances for the particular scene in cloud-free conditions. These estimates should account for the viewing and illumination conditions as well as variations in the atmospheric components and surface properties. Theoretical, empirical, or combinations of theory and observations can be used to provide these estimates. Atmospheric absorption and emission for each channel is taken into account using a radiative transfer model that employs the correlated k -distribution approach to determine the spectral optical depths within each layer of the atmosphere [2]. The atmospheric soundings of temperature, humidity, and ozone are taken from hourly interpolations of the European Center for Medium-range Weather Forecasting (ECMWF) 6-hourly reanalyses. Nominal loadings of various absorbing trace gases are also used to complete the spectral absorption calculations.

Clear-sky reflectance

Theoretical reflectance models for the snow surface at 0.65, 1.6, and 3.75 μm were developed from calculations using an adding-doubling radiative transfer model [3]. The snow surface was approximated as a layer comprising randomly oriented, hexagonal ice crystals having a length to width ratio, L/D of 750 $\mu\text{m}/160 \mu\text{m}$ [4] with an optical depth of 1000. The surface snow reflectances for 0.65, 1.6 and 3.75 μm are corrected to obtain the TOA reflectance using Rayleigh scattering and the proper absorption for each channel. Each snow bi-directional reflectance model consists of 21 solar zenith angle (θ_o) bins, 21 view zenith angle (θ) bins, and 25 relative azimuth angle (ϕ) bins. For each MODIS pixel, given a set of (θ_o , θ , ϕ), the clear-sky reflectance $\rho_{cs1.6}$ and $\rho_{cs3.7}$ are computed from the models [5].

Clear-sky temperature

Snow surface emissivities were computed for each channel with the same approach used for reflectance. The 3.75- μm snow emissivity is a function of view zenith angles. The expected clear-sky TOA temperatures over snow at 3.75 and 11 μm are predicted in the following manner. The value of $\rho_{cs3.7}$ is used with the hourly interpolated ECMWF 3-hourly surface skin temperatures, the 3.75- μm surface emissivities and the atmospheric absorption corrections to derive the expected clear-sky temperature at 3.75 μm ($T_{cs3.7}$). The expected clear-sky 11 and 12- μm temperatures, T_{cs11} and T_{cs12} , are derived in a similar manner without the reflectance component because there is no solar radiation and the atmospheric emission in the infrared window is minimal in clear polar regions.

2.2 Daytime polar mask using NIR and SIR models

The current CERES cloud mask consists of a set of cascading threshold tests that ultimately define a pixel as clear, cloudy, to-be-determined (TBD), or bad data [6]. Cloudy pixels are sub-classified as strong, weak, or no retrieval. Sub-categories for clear pixels include strong, weak, snow, aerosol, smoke, fire, glint, or shadow. Because the initial CERES cloud retrievals were performed using the Visible and Infrared Scanner (VIRS) data on board the Tropical Rainfall Measuring Mission (TRMM) which covers between 37°N and 37°S latitudes, snow cover was not a central focus of the mask. With MODIS data taken frequently over the poles, it is necessary to ensure that the mask is operating accurately.

Figure 1 summarizes the daytime (defined for times when $\theta_o \leq 82^\circ$) cloud detection process. It employs a decision tree type structure to analyze MODIS five-channel sensor data for 0.65, 1.6, 3.75, 11, and 12 μm together with the predicted clear sky values to identify clouds and snow and ice. The first step is to detect obvious clouds by comparing the observed BTD_1 ($T_{3.7} - T_{11}$) against a threshold. A positive cloud detection is automatic if BTD_1 exceeds 18 K. Otherwise, a second tier of tests that consists of NIR and SIR tests is applied. The NIR test compares the difference between observed 1.6- μm reflectance $\rho_{1.6}$ and $\rho_{cs1.6}$ with the standard deviation of the 1.6- μm clear-sky map ($\sigma_{1.6}$). If a pixel passes the NIR test, then the $\text{NIR_Flag} = 1$, otherwise, the $\text{NIR_Flag} = 0$. The SIR test compares the difference between the observed BTD_1 and the expected clear-sky BTD_{1cs} with one standard deviation $\sigma_{3.7-11}$ that is currently constant at 3 K. $\text{SIR_Flag} = 1$ if the pixel passes SIR test, otherwise, the $\text{SIR_Flag} = 0$. The pair of tests results in four possible conclusions that are used to select the additional tests to arrive at the final scene classification. The subsequent

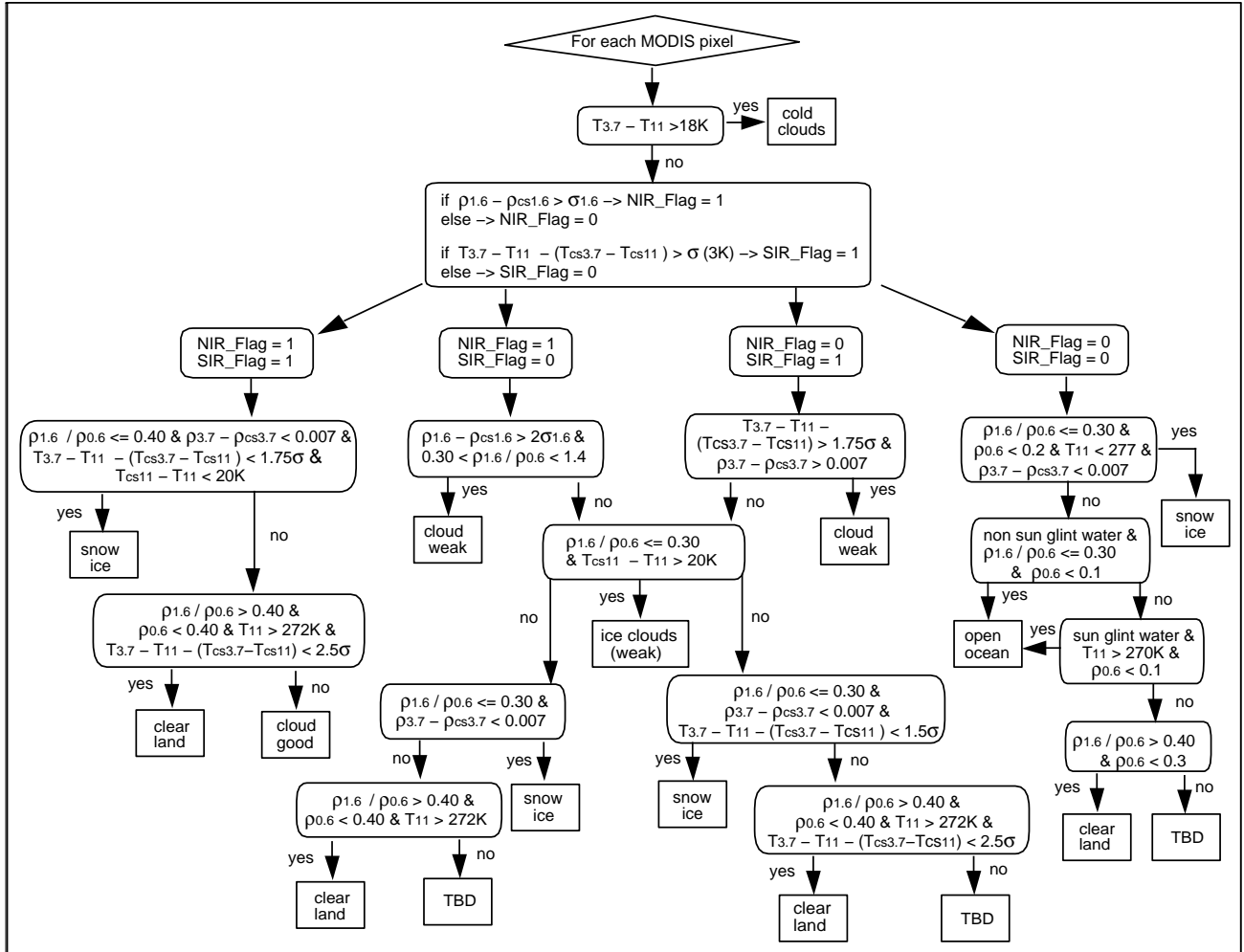


Fig. 1. Daytime polar cloud mask.

tests utilize the ratio of the 1.6 and 0.65- μm reflectances ($\rho_{1.6} / \rho_{0.6}$), the difference between observed 3.75- μm reflectance and its expected clear-sky value ($\rho_{3.7} - \rho_{cs3.7}$), the difference between the predicted clear-sky TOA temperature and the observed 11- μm brightness temperatures ($T_{cs11} - T_{11}$), 0.65- μm reflectances, etc. The logic is to first detect any type of clouds including middle and low clouds, ice-clouds, and thin cirrus clouds. The cloud decision is also assigned different confidence levels indicated by the modifiers strong or weak. If a cloudy scene is ruled out, then the pixel continues down the decision tree to determine if snow or ice is present. Failing the snow-ice tests, the scene will then be classified as clear land or open ocean or as unknown (TBD).

2.3 Nighttime and twilight polar mask

During nighttime (defined for times when $\theta_o > 82^\circ$), detecting clouds over snow and ice surfaces is challenging because the satellite observations are limited to infrared channels only and low clouds, inversions, and shallow lapse rates are often present. The CERES nighttime polar mask utilizes the MODIS-observed BTD_1 , BTD_2 ($T_{3.7} - T_{12}$), BTD_3 ($T_{8.5} - T_{11}$), and BTD_4 ($T_{6.7} - T_{11}$) to detect various clouds while relying on the IGBP (International Geosphere Biosphere Program) ecosystem map and daily snow and ice maps from the National Snow and Ice Data Center to determine the locations of snow and ice surfaces. MODIS frequently observes the Earth in “twilight” conditions (defined for times

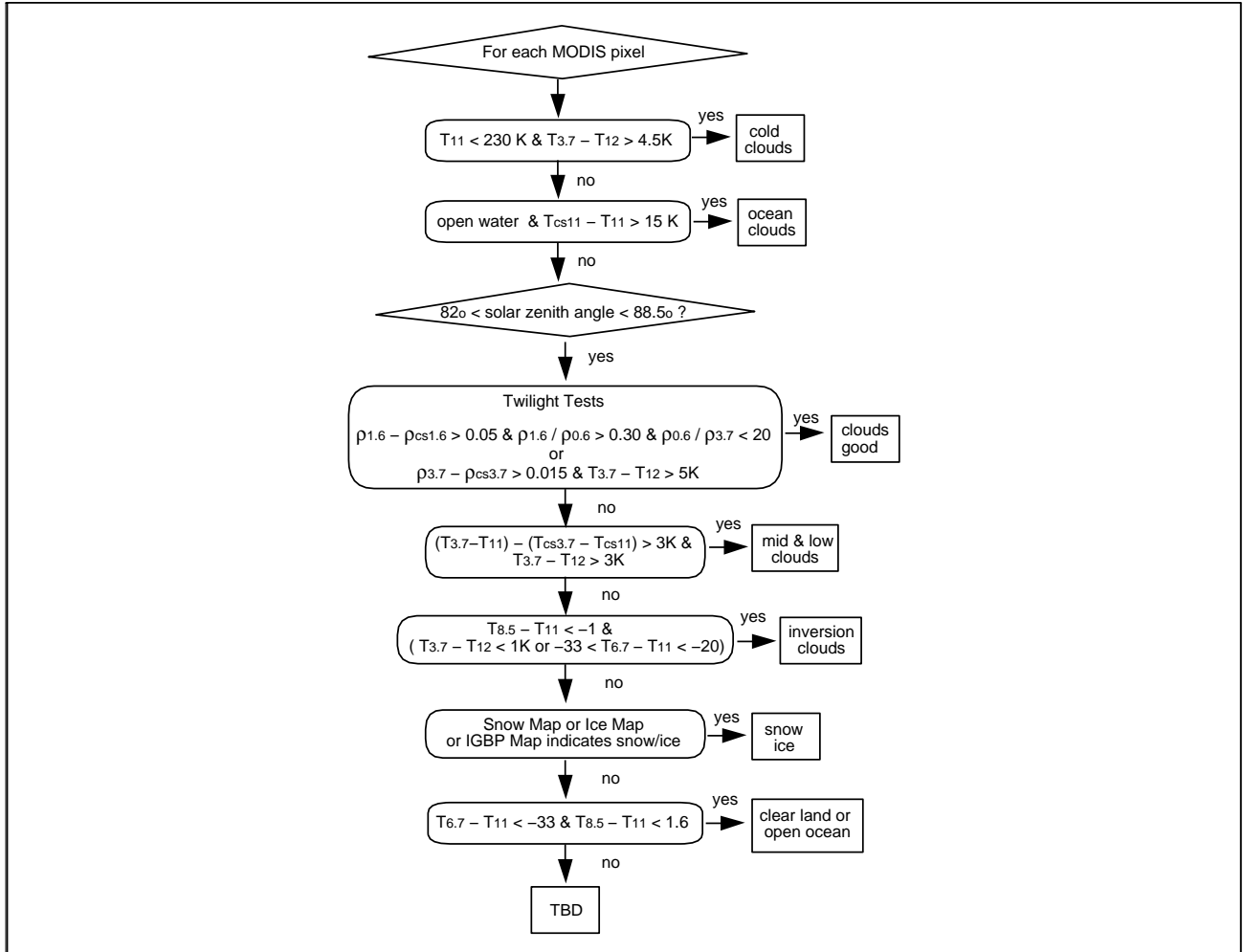


Fig. 2. Nighttime and twilight polar cloud mask

when $82^\circ < \theta_o < 88.5^\circ$) at high latitudes, especially during spring and autumn seasons. A separate cloud detection scheme using the reflected solar components at 1.6 and 3.75 μm was developed for the regions in twilight.

Figure 2 shows the nighttime and twilight cloud detection process. The decision tree consists of a series of cloud tests that identify different types of cloud signatures in the multispectral satellite data. If clouds are detected at any time in the sequence, the process is completed. Otherwise, the testing continues down the decision tree until reaching a final classification. Similar to the daytime procedure, the obvious clouds are first filtered out by comparing the observed T_{11} and BT_{D2} against empirical thresholds. The difference between T_{11} and T_{11cs} is used to detect clouds over open ocean when no sea ice present. Then, the twilight cloud tests are applied if appropriate, followed by inversion clouds detection and snow-ice surface determination. If no cloud or snow-ice decision is made, the algorithm returns TBD.

3. RESULTS

The polar scene identification algorithms were applied to 5-minute swaths of MODIS data taken between February and July 2001 over the Arctic Ocean and surrounding areas and over Antarctica and adjacent coastal areas. Each 5-minute swath consists of 2030 scan lines that are 1-km apart. Each scan line contains 1354 1-km pixels. The data were sampled every other pixel and scan line to achieve an effective resolution of 2 km.

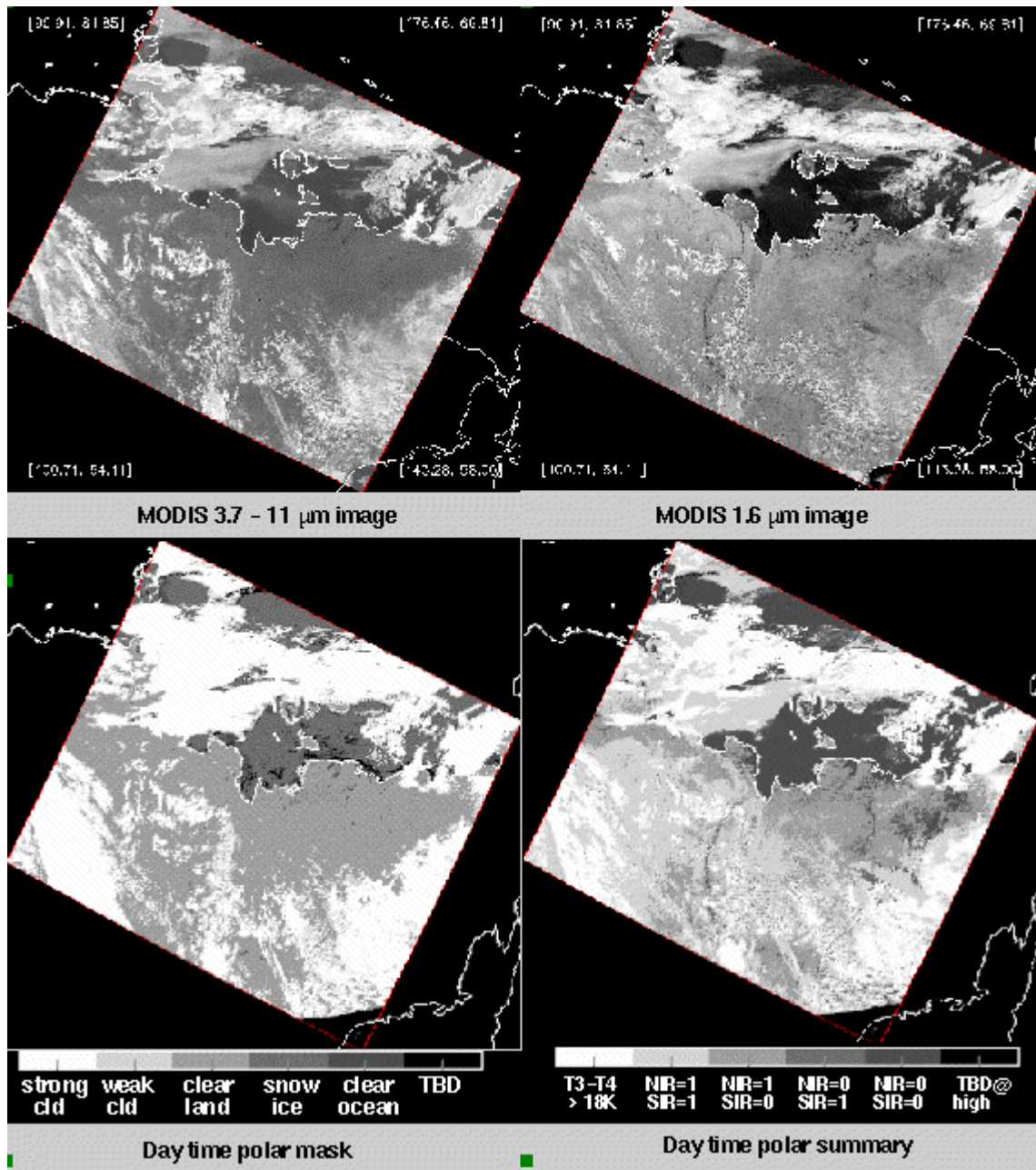


Fig. 3. Daytime polar cloud mask applied to MODIS data over Siberian Sea and Laptev Sea, 0320 UTC, 4 July 2001.

3.1 Daytime Arctic Ocean

Figure 3 shows the results of the mask algorithm applied to a daytime swath taken 4 July 2001 over the east Siberian and Laptev Seas and over part of northern Siberian. The upper two panels are MODIS images of BTD_1 and $\rho_{1.6}$ reflectance. Both seas are frozen appearing as darker gray in the BTD_1 and black in the 1.6- μm images because snow and ice are not very reflective in the 1.6 and 3.7- μm channels. The snow-free land over Siberian (at the lower portion of the images) is more reflective indicated as lighter shades of gray in both images. The whitish colors correspond to various types of clouds. The polar mask results are shown at the bottom left panel. Almost all the clouds in this swath

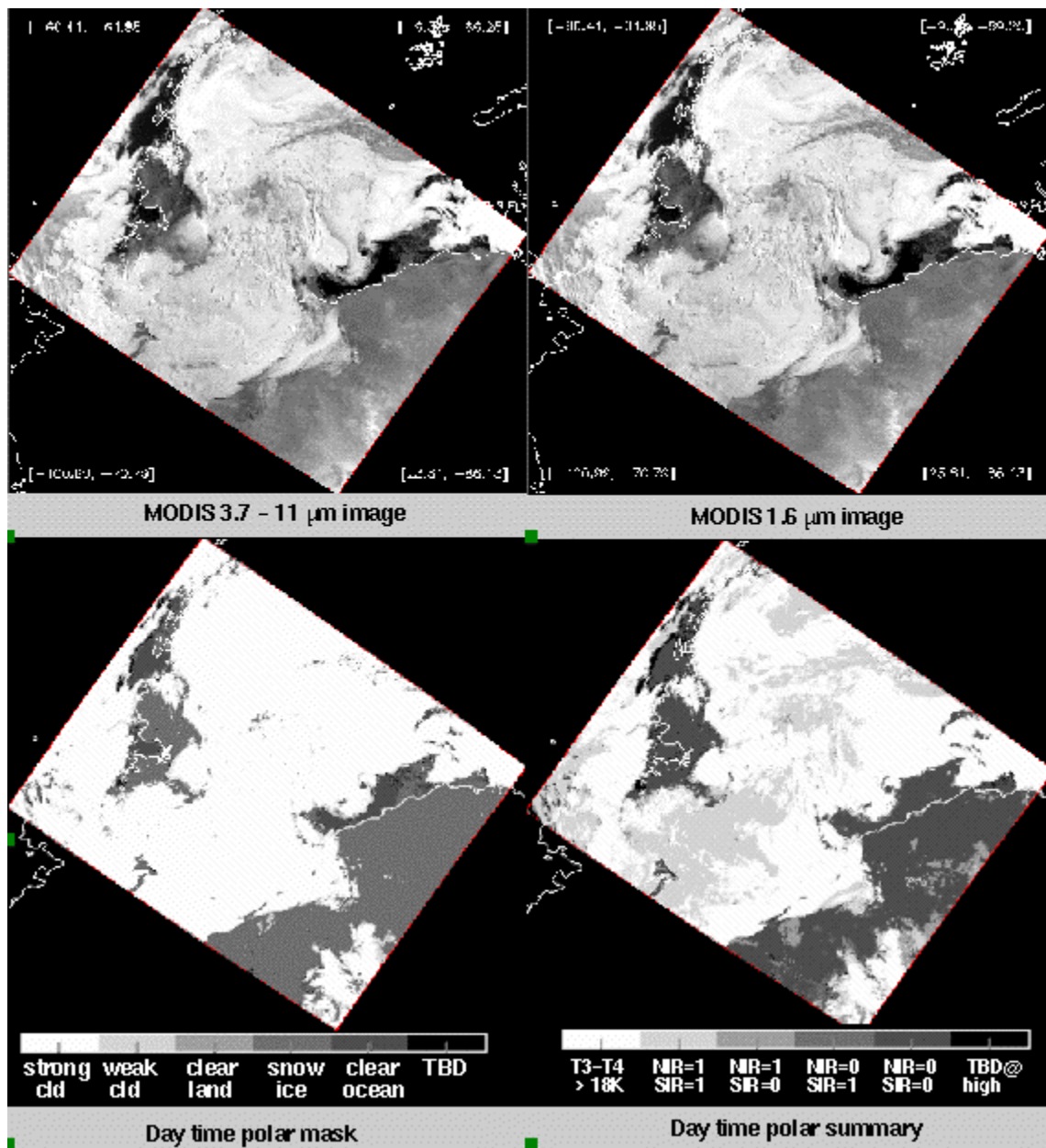


Fig. 4. Daytime polar cloud mask applied to MODIS data over Antarctic Peninsula, 1155 UTC, 14 February 2001.

are classified as strong clouds (white). The light gray areas are identified as clear land and the darker gray areas towards the north are sea ice retrieved by the polar mask. The mask results agree very well with a visual interpretation of the satellite images. The bottom right panel is the polar mask summary. It is designed to keep track which branch of the cloud decision tree made the final classification.

3.2 Daytime Antarctic

The daytime polar cloud mask results over the Antarctic Peninsula for 14 February 2001 are shown in Fig. 4. Cold clouds covered most of the Weddell Sea and the Ice Shelf shown in BTD_1 and 1.6- μm images. There are patches of open water at the two sides of Weddell Sea shown in black from MODIS images. The clouds, snow and ice surfaces, and the clear ocean are well represented in the resulting polar mask. The white color in the polar summary corresponds

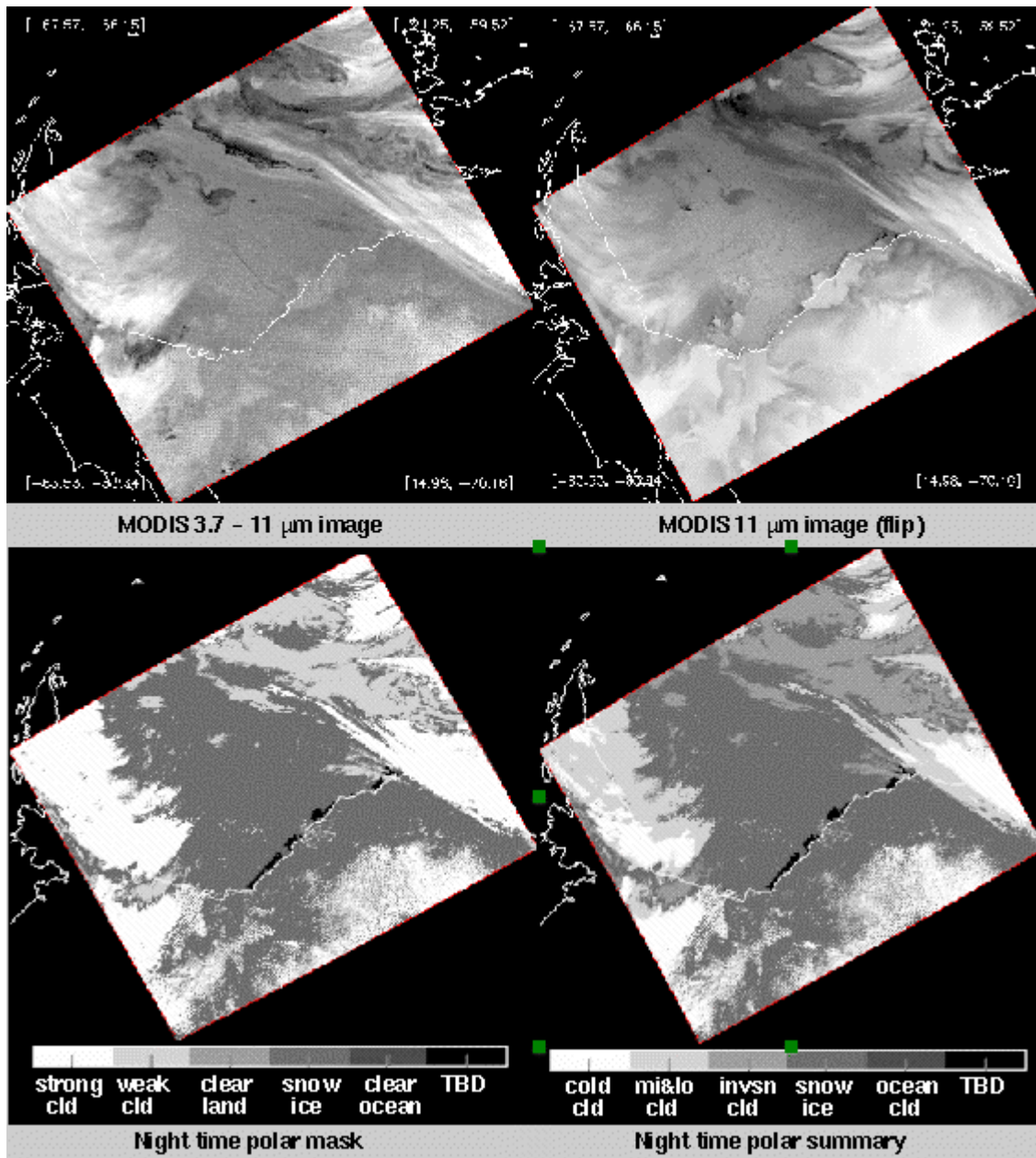


Fig. 5. Nighttime polar mask applied to MODIS data over Weddell Sea, 0230 UTC, 4 July 2001.

to the areas where BTD_1 greater than 18 K; the light gray areas are the regions where the NIR and SIR tests both detect clouds; while the darker gray is where both NIR and SIR tests detect no clouds and the other tests indicate snow ice surfaces.

3.3 Nighttime Weddell Sea

Figure 5 shows a nighttime MODIS swath taken on 4 July 2001 at Weddell Sea and surrounding areas. Cirrus clouds are present at the two edges of the swath shown in white in the BTD_1 and reversed 11- μ m images. Sea ice and the ice shelf are shown in gray in the middle of the MODIS images. In general, the nighttime polar mask results agree fairly well with visual interpretation of the MODIS images. The black line crossing the center of polar mask is TBD

corresponding to the uncertainties in the snow and ice maps. The nighttime polar summary indicates which group of the tests are used to classify each pixel.

3.4 Twilight Arctic Ocean

Figure 6 shows a subset of a 5-minute MODIS swath mostly in twilight illumination (see the solar zenith angles at bottom right panel). The BTD₂ and 1.6- μm reflectance images are shown on the top row. The twilight cloud algorithm makes use of the reflected solar component, combined with infrared information, to detect clouds. The twilight polar mask results are very consistent with the MODIS images in this case.

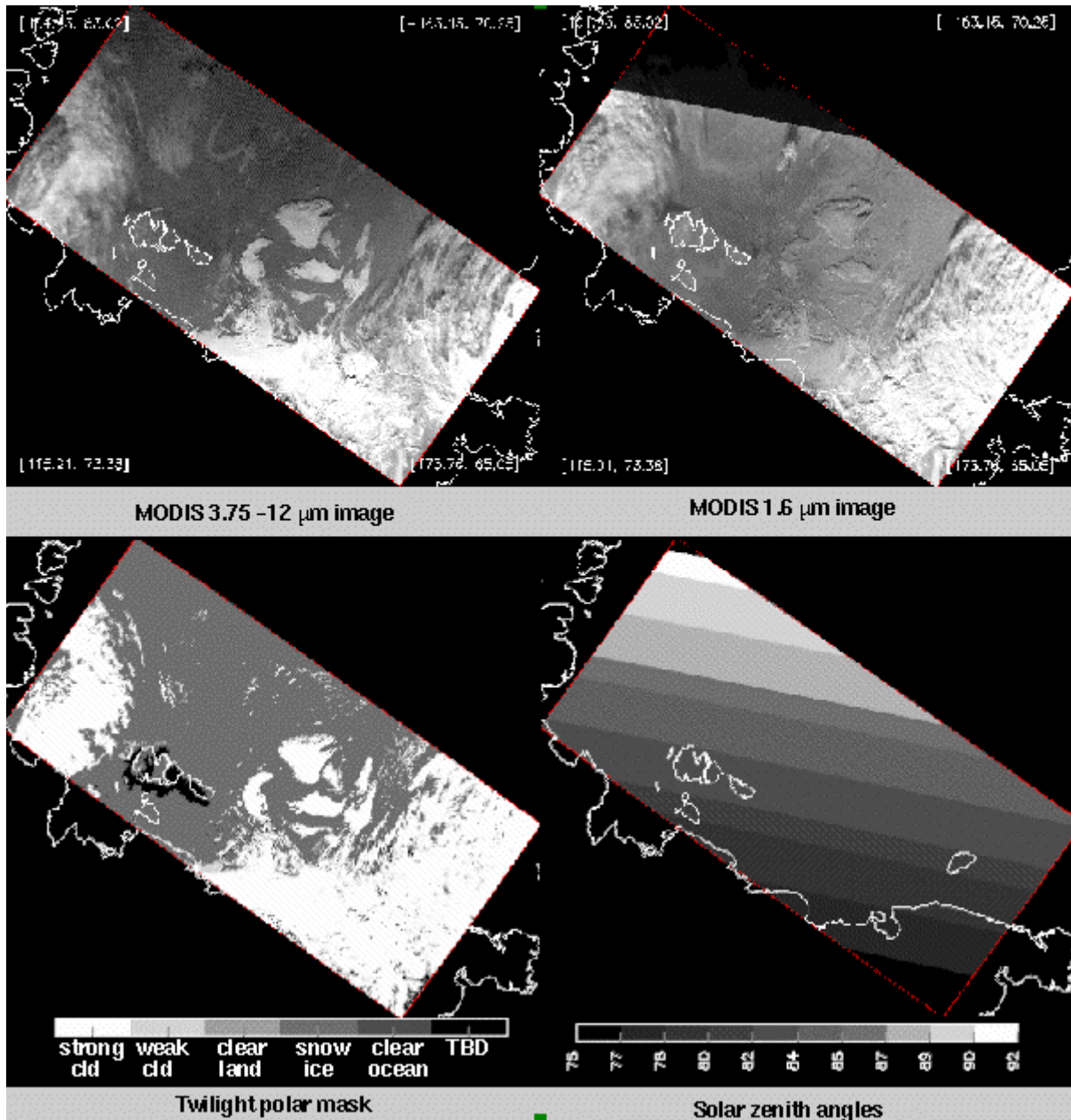


Fig. 6. Twilight polar cloud mask applied to MODIS data over the Arctic Ocean, 0215 UTC, 1 March, 2001.

3.5 Comparison of MODIS-observed snow reflectance with theoretical models.

The daytime polar scene identification algorithm was applied to 29 MODIS 5-minutes swaths over the Arctic regions and 21 swaths over the Antarctic regions taken from January to July 2001. The mean values of 0.65, 1.6, and 3.75- μm reflectance for all of the clear snow pixels identified by the polar mask were computed for each 5° interval of viewing zenith angle VZA to determine how closely the resulting values compared with the model results. The relative azimuth angles in all of these cases vary from 40° to 140° , so there are no pixels with geometry near the principal solar plane. The solar zenith angles range between 56° and 82° .

Figure 7 shows the 0.65- μm MODIS observed reflectance and snow ice bi-directional model as a function of VZA. Over the Antarctic, the model is closer to the observations than over the Arctic, where the mean model reflectance is about 10-12% higher than the observations. This discrepancy is probably caused by the different characteristics of snow and sea ice between Antarctic and Arctic. In the northern hemisphere spring and summer, snow tends to melt from top down while the reverse is true for the southern hemisphere. Once melting begins in the Arctic, the surface contains a mixture of melt ponds, snow, and ice that typically reduces the reflectance compared to a pure snow surface. In the future, different size of snow grains may be used to develop separate theoretical snow reflectance models for each pole.

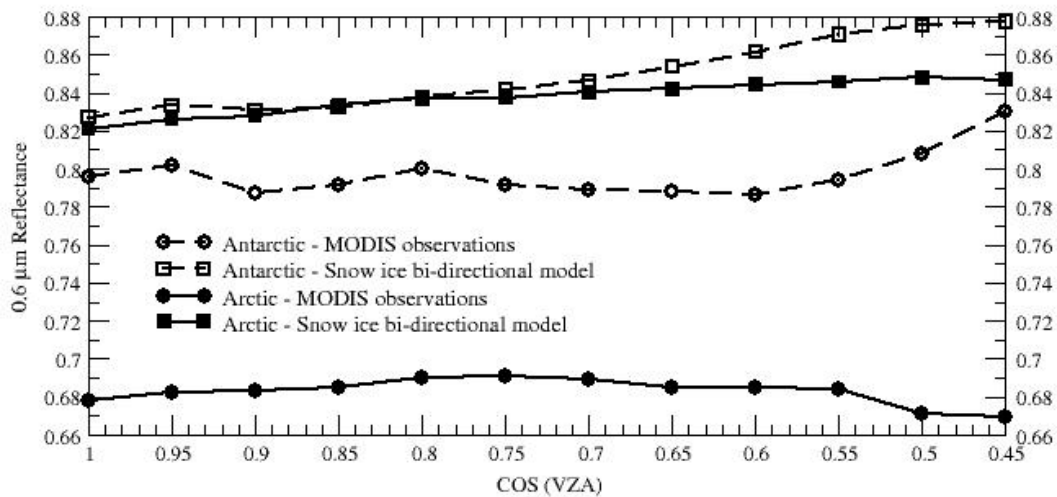


Fig. 7. Comparison of the mean MODIS and modeled 0.65- μm snow reflectances.

A comparison of the model and observed NIR snow reflectances is shown in Fig. 8. for the same dataset. The 1.6- μm snow bi-directional model shows good agreement with the mean MODIS observations for the Arctic and Antarctic regions; both increase as the view zenith angles increase. In the Antarctic, the model values are 5-10% greater than the observed reflectances, while the agreement is very close for most VZA's in the Arctic. The trend of the observed 1.6- μm agrees with other studies. Airplane measurements of the reflectance over snow-covered tundra and sea ice at $\theta_o = 65^\circ$ showed that the 1.6- μm reflectance increased monotonically from a mean value 0.12 at nadir to 0.14 at 30° up to 0.40 at 70° ($\cos\theta = 0.34$).

Comparisons of the mean 3.75- μm MODIS and modeled snow reflectances are shown in Fig. 9. The modeled and observed reflectances share the same trend, but the model values are about 9% higher at nadir and 35% higher at VZA = 63° . One possible source of the model-observation disagreements at 3.75 μm is the uncertainty in the calibration. The larger part of the bias may be due to the crystal size used in the calculations. A previous study [5] found relatively good agreement between the 3.75- μm reflectance model used here and well-characterized clear polar ice scene reflectances, but that small amounts of haze or fog can dramatically increase the 3.75 μm reflectance. Therefore, any scenes containing haze or fog would cause overestimates of the reflectances relative to a model value without haze. Surface

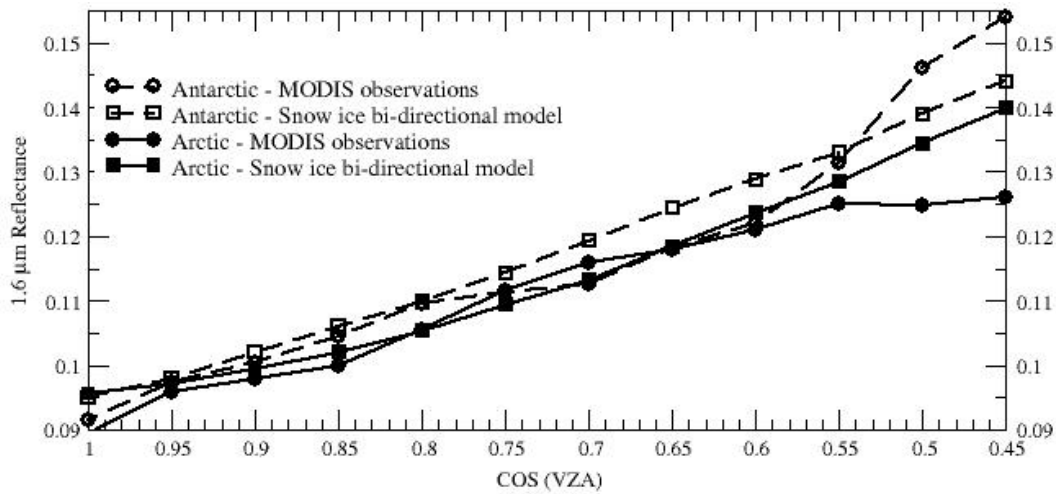


Fig. 8. Comparison of mean MODIS and modeled 1.6- μm snow reflectances.

observations [8] revealed that erosional features in the snow, sastrugi, in areas like the Antarctic cause more absorption of visible wavelengths by the snow, an effect that may also reduce the reflectance of snow at 1.6 μm as the VZA increases. Sastrugi have preferred orientations and therefore would introduce asymmetry into a bidirectional reflectance pattern. Thus, the bias seen here may in part be due to surface topographical effects.

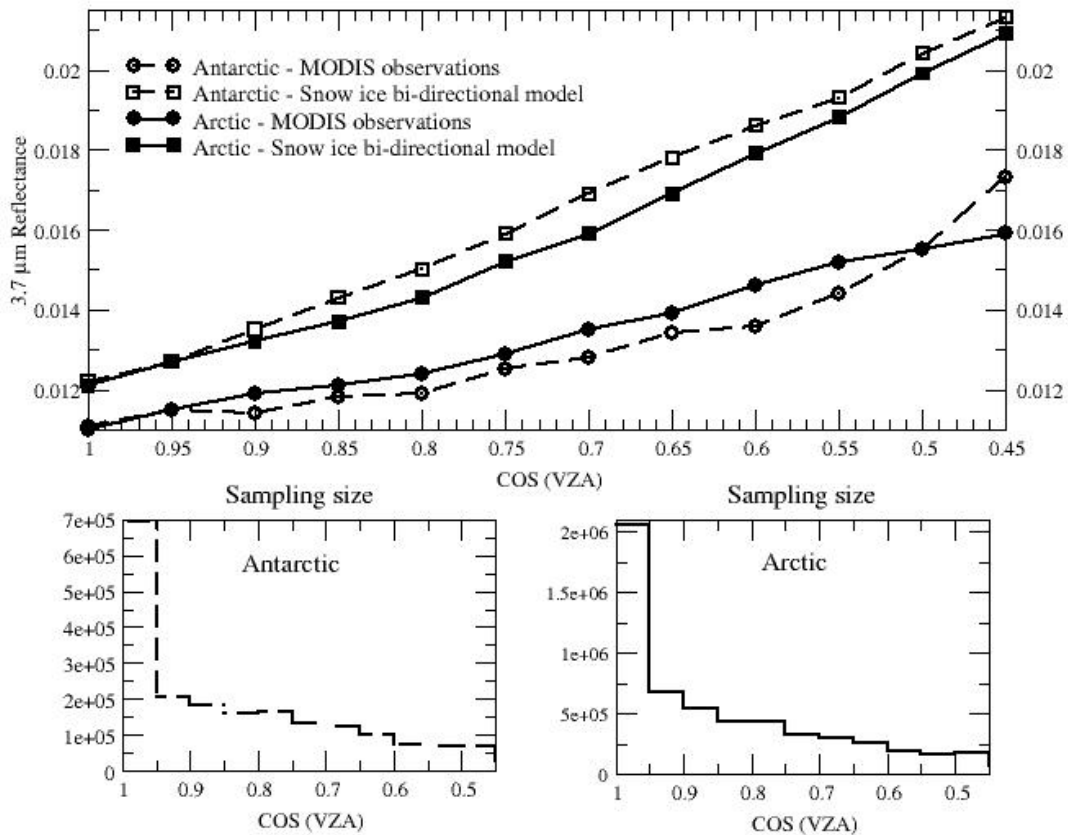


Fig. 9. Comparison of mean MODIS and modeled 3.75- μm snow reflectances.

4. CONCLUDING REMARKS

The CERES polar cloud and snow identification algorithm was developed and applied to the MODIS data. The results show fairly good agreement with visual interpretation of the satellite images and with the models. Additional study is needed to develop more realistic snow reflectance patterns at the various wavelengths. More rigorous validation efforts are also required to ensure that the masks are detecting cloud cover accurately in all conditions. Surface observer data, both instantaneous and climatological will be compared to the operation CERES results. Comparisons of the cloud fractions derived from the December 2000 and June 2001 MODIS data with the surface climatology [9] indicate that the daytime mask is producing very reasonable cloud amounts over the Arctic. The initial nighttime results appear less accurate than the daytime values as expected. More detailed studies using the Atmospheric Radiation Measurement Program active sensors at Barrow, AK will be extremely valuable for more objective validation of the classifications and for developing necessary improvements to the algorithms.

ACKNOWLEDGEMENTS

This research was supported by the NASA Earth Sciences Enterprise CERES Project and Environmental Sciences Division of the DOE ARM Program Interagency Agreement DE-AI02-97ER62341.

REFERENCES

1. Wielicki, B. A., et al., Clouds and the Earth's Radiant Energy System (CERES): Algorithm overview. *IEEE Trans. Geosci. Remote Sens.*, **36**, 1127-1141, 1998.
2. Kratz, D.P., The correlated k -distribution technique as applied to the AVHRR channels. *J. Quant. Spectrosc. Radiat. Transfer*, **53**, 501-517, 1995.
3. Minnis, P., Y. Takano, and K.-N. Liou, Inference of cirrus cloud properties using satellite-observed visible and infrared radiances, Part I: Parameterization of radiance fields. *J. Atmos. Sci.*, **50**, 1279-1304, 1993.
4. Takano, Y. and K. N. Liou, Radiative transfer in cirrus clouds: I. Single scattering and optical properties of oriented hexagonal ice crystals. *J. Atmos. Sci.*, **46**, 3-20, 1989.
5. Spangenberg, D. A., V. Chakrapani, and D. R. Doelling, P. Minnis, and R. F. Arduini, Development of an automated Arctic cloud mask using clear-sky satellite observations taken over the SHEBA and the ARM NSA sites. *Proc. AMS 6th Conf. Polar Meteorol.*, San Diego, CA, May 14-28, 2001.
6. Trepte, Q., Y. Chen, S. Sun-Mack, P. Minnis, D. F. Young, B. A. Baum, and P. W. Heck, Scene identification for the CERES cloud analysis subsystem. *Proc. AMS 10th Conf. Atmos. Rad.*, Madison, WI, June 28 – July 2, 169-172, 1999.
7. Arnold, G. T., S.-C. Tsay, M. D. King, J. Y. Li, and P. F. Soulen, Airborne spectral measurements of surface-atmosphere anisotropy for Arctic sea ice and tundra. *Intl. J. Rem. Sens.*, submitted 2000.
8. Warren, S. G., R. E. Brandt, and P. O'R. Hinton, Effect of surface roughness on bidirectional reflectance of Antarctic snow. *J. Geophys. Res.*, **103**, 25,789-25,807, 1998.
9. Minnis, P., D. F. Young, B. A. Wielicki, S. Sun-Mack, Q. Z. Trepte, Y. Chen, and P. W. Heck, A global cloud database from VIRS and MODIS for CERES. *Proc. SPIE Conf. Optical Remote Sensing of the Atmosphere and Clouds III*, Hangzhou, China, Oct. 23-27, 2002.